Local Variance and Homogeneity of White Matter Microstructure Provides a Practical Method to Assess Focal and Multifocal Neuronal Disease in Individuals Using Magnetic Resonance Diffusion Tensor Imaging

Abigail Hentel

Abstract:

Introduction: Diffusion tensor imaging (DTI) can be used to quantify white matter integrity. However, common metrics such as fractional anisotropy (FA) are sensitive to sequence parameters and scanner hardware. This paper proposes a new metric to assess DTI that may be insensitive to sequence parameters and scanner hardware.

Methods: DTI was collected on 40 normal healthy adults on up to three different magnetic resonance imaging (MRI) scanners each running a unique DTI sequence. FA of 61 regions of interest (ROI) within 6 tracts were measured and analyzed for differences based on scanner/sequence type. A local variance measure was also computed for each ROI.

Results: FA was significantly different ($p<0.05$) for each scanner/sequence group for all white matter tracts. No statistically significant differences were found using the local variance measure ($p > 0.05$ for all ROIs).

Discussion: It is invalid to combine or compare FA from DTI data sets from different scanners and/or sequence parameters. In contradistinction, the local homogeneity measure appears insensitive to these variations suggesting the possibility to use this approach to either combine DTI data across vendors and sequence types or interpret individual DTI data sets without a comparative normative database or prior DTI scan.

1. Introduction

Throughout a lifespan, the human brain is constantly changing and developing. White matter, composed of myelinated axons, forms tracts throughout the brain that transmit nerve impulses to convey information. These white matter pathways are critical for cognitive function and can be injured in trauma or altered from various neurodegenerative disorders, medications, or neuropsychological conditions.[1] Neurological disorders and diseases affecting these white matter tracts account for 1.5 trillion dollars of the United States economy per year[2]. In particular, traumatic brain injury has become a major cause of long term disability around the world[3,4]. TBI alone accounts for 30% of all injury deaths and in 2013 lead to 50,000 deaths[4]. Unlike many other neurological disorders, mild TBI, which accounts for over 80% of all TBI, poses a diagnostic imaging challenge.

As a result, reliable assessment of white matter tracts is critical for providing diagnosis, prognosis, or monitoring progression of disease and treatment. The hallmark of mild TBI is traumatic axonal injury, which manifests as microstructural shear injury of white matter pathways[5]. The microstructural changes in mild TBI are typically beyond the sensitivity of CT and conventional MRI, which operate at macroscopic resolutions. While CT and, more so, MRI can detect microhemorrhages, which serve as a proxy for axonal injury, numerous studies document that both techniques grossly underestimate the true extent of axonal injury and number of microhemorrhages fail to correlate with cognitive function or TBI outcomes.[6–9]

Unlike conventional MRI, magnetic resonance diffusion tensor imaging (DTI) is very sensitive to changes in white matter microstructure[10,11]. DTI measures the passive diffusion of water molecules which are influenced by the local integrity and coherence of white matter. Axonal injury perturbs the normal diffusion and can be quantified by the loss of anisotropy or mean diffusivity. DTI can be quantified through multiple metrics, which describe the three-dimensional profile of diffusion including fractional anisotropy (FA), mean diffusivity (MD), axial diffusivity (AD), and radial diffusivity (RD)[8]. FA most directly appears to reflect the microstructural integrity of the white matter tracts in the brain, and FA maps can be used to see the anatomical structure of the brain. Another common metric, MD, describes the average diffusion coefficient throughout the tract.

Less commonly used are RD and AD. RD appears more specific to white matter myelin integrity while AD appears more sensitive to axonal loss[12].

DTI already has been proven as a biomarker for many neurological disorders and diseases including Alzheimer's Disease[13–15], bipolar disorder[16–18], schizophrenia[19], and traumatic brain injury[20–24].

Normal aging is known to affect the white matter composition in the brain. In general, white matter volume and integrity increases in the brain from infancy through the second and third decade of life beyond which it begins to plateau and slowly atrophy later in life[25]. As a result, DTI metrics of white matter integrity have been shown to vary with age. Childhood through early adulthood is manifested by increasing fractional anisotropy and decreasing mean diffusivity[26–28]. In contradistinction, late adulthood is characterized by decreased FA and increased MD[29–31].

Additionally, DTI is influenced by hardware and pulse sequence parameter selection. There have been numerous studies focusing on different variables such as the vendor, magnetic field, and inter-site versus intra-site scanners. While DTI differences are seen between scanners from different vendors, even two scanners of the same make and model have slight variations that can yield different DTI results. When comparing inter versus intra site scanners, it is found that inter site scans on the same machine have a higher variability than intra site scans[32]. This can be due to the machines at different locations being operated slightly differently and other slight variations depending on the location. Vollmar et al. 2010 found a 40% difference between inter versus intra site, the higher variability being in the inter site data[33]. The manufacturing companies have tried to limit the variability between sites by constant software updates, but these software updates can cause more harm than benefit, as stated by Vollmar et al in 2010[33]. More dramatic differences are seen in scanners of varying field strength, although, 3.0 T MRI machines have been found to produce smaller variances for MD and FA compared to a 1.5 T machine[34].

These influences upon DTI acquisition and measurement are important because they pose a practical problem for assessment of patient data. Typically, individual DTI data is compared to normative databases of DTI data acquired on the same scanner hardware, pulse sequence parameters, and software version. Collection of these

normative databases is both challenging and costly. Hardware and software upgrades can yield previously collected DTI data obsolete. Data from multiple scanners within the same institution or multiple sites cannot be combined due to differences in scan measurements. Furthermore, it can be impractical to collect enough normal healthy subjects to determine the true range of normal variability within each age range as individuals ought to be compared to their own age group given the evolution of white matter composition with age.

These challenges and limitations prevent DTI from being used clinically. While discrete values of DTI metrics such as FA and MD vary with scan parameters and hardware, it is likely that these variations are systemic through all tracts and along the course of any individual tract. Given mild TBI typically manifests as focal or multifocal traumatic axonal lesions causing local changes in FA and MD, it may be possible to quantify the local homogeneity of the tract, a metric that would be scan parameter and hardware independent.

The goal of this research is to test the homogeneity of the DTI metrics of white matter tracts in normal healthy individuals performed on varying hardware and scan parameters to verify if these factors influence DTI measurements and secondly determine if local homogeneity is independent of these hardware and parameter variations. Finally, DTI from a subject with a known mild to moderate traumatic brain injury is assessed using this local variance measure to determine if this metric may be sensitive to focal traumatic axonal injury lesions.

2. Methods

The data was retrospectively collected from an anonymized normative database collected under a Weill Cornell Medical College Internal Review Board approved study protocol in which normal healthy adults voluntarily agreed to undergo a non-contrast MRI scan including DTI on up to three different scanners at our institutions.

Subjects included healthy adults without history of head trauma, prior or ongoing neurological or neuropsychological condition, brain surgery, or have had a contraindication to undergo MRI. A total of 40 subjects participated, consisting of 23 males, 17 females with age ranging from 23 to 79 years (mean = 40 years, SD 17 years). Subjects were scanned on up to three of the following scanners: 3 Tesla (3T) GE Signa

EXCITE (GE Healthcare, Waukesha, WI); a 1.5 T GE Signa EXCITE scanner; or a 3T Siemens (Munich, Germany). Both GE scanners were equipped with an 8-channel phased-array head coil. The Siemens scanner was equipped with a 32-channel head phased-array head coil.

In addition to conventional clinical sequences which were screened by board certified neuroradiologists, whole brain axial diffusion tensor imaging using echoplanar multislice single-shot spin echo was acquired and analyzed as part of this manuscript using the following protocols:

- 33-Direction 1.5T GE DTI, TE=109 ms, TR=10 s, 33 diffusion-encoding directions at b=1000, 1 b=0 volume, FOV 240, 256 x 256 matrix, 2.5 mm slice thickness.
- 55-Direction 3.0T GE DTI, TE=109 ms, TR=8 s, 55 diffusion-encoding directions at b=1000, 1 b=0 volume, FOV 230, 128 x 128 matrix zero-filled to 256 x 256, 1.8 mm slice thickness.
- 64-Direction 3.0T Siemens DTI, TE=100ms, TR=12 s, 64 diffusion-encoding directions at b=1000, 1 b=0 volume, FOV 240, 128 x 128, 2.0 mm slice thickness.

Of the 40 subjects, 30 subjects underwent scanning on the 3T GE scanner (55-direction DTI sequence); 40 subjects were scanned on the 3T Siemens scanner (64-direction DTI sequence); and 11 subjects were scanned on the 1.5 T GE scanner (33-direction DTI sequence).

2.1 DTI post-processing and analysis

DTI data was co-registered to each subject's respective b=0 image volume followed by eddy current correction and motion correction performed using the fMRIB Diffusion Toolbox (part of FSL; www.fmrib.ox.ac.uk/fsl)[35]. The diffusion tensor was computed using DTIfit from FSL to obtain FA maps, Mean Diffusivity (MD) maps, and eigenvalue maps.

For each DTI scan, white matter pathways were identified and 3D space was analyzed using the Reproducible Objective Quantification Scheme (ROQS)[36]. This is a semi-automated technique operating in the native image space using user input as seeds

which can identify tracts in three dimensions and selects cross-sectional 2D regions of interest (ROI). For each subject, the corpus callosum (CC), corticospinal tract (CST), cingulum bundle (CB), superior longitudinal fasciculus (SLF), anterior corona radiata (ACR), and uncinate fasciculus (UF) were identified and analyzed in the following manner:

For the CC, 15 evenly spaced coronal cross section ROIs starting anteriorly from the genu extending posteriorly to the splenium were analyzed.

For the CST, 16 total axial cross section ROIs were analyzed spanning superiorly from the centrum semiovale to the superior corona radiata through the posterior limb of the internal capsule.

For the CB, a total of 8 evenly spaced cross-sectional ROIs spanning anteriorly to posteriorly were analyzed.

For the SLF, a total of 8 evenly spaced cross-sectional ROIs spanning anteriorly to posteriorly were analyzed.

For the ACR, a total of 6 evenly spaced cross-sectional ROIs spanning anteriorly to posteriorly were analyzed.

For the UF, a total of 8 evenly spaced cross-sectional ROIs spanning anteriorly to posteriorly were analyzed.

Each ROI yielded mean FA, MD, each eigenvalue, and the respective standard deviations.

2.2 Statistical analysis

The average FA score for the cross-sectional ROIs across subjects were computed for the 55-direction, 64-direction, and 33-direction groups separately and plotted. Given the non-Gaussian distribution of subjects, nonparametric tests were used. The Wilcoxon-Mann-Whitney test was used to compare each cross-sectional ROI to test for statistical difference between the 55 vs 64- direction groups, the 55- vs 33-direction groups, and the 64- vs 33-direction groups. All p-values were two-sided with statistical significance evaluated at the 0.05 alpha level. Analyses were performed using SPSS Version 25.0 (IBM Inc., Armonk, NY). Subjects scanned on multiple platforms were treated independently.

A measure of local variance was also computed for each ROI by measuring the in-plane variance of the FA and averaging it with the out-of-plane variance generated by the ROIs measured from the previous and subsequent slices (see Fig 1). This local variance measure was averaged for each group separately and compared using the Wilcoxon-Mann-Whitney test to test for statistical differences.

3. Results

Figures 2-7 illustrate the average FA for each cross-sectional ROI for every tract for the 3 groups of data, the 55-direction 3T GE group, the 64-direction 3T Siemens group, and the 33-direction 1.5T GE group. This analysis, mimicking typical ROI analysis of DTI data demonstrates variability among the three groups. Statistical differences among the groups vary based on both white matter pathway and also location within each white matter pathway. These statistical differences are highlighted in Tables 1-6, which report p-values for comparison of each cross-sectional ROI between the groups.

In figure 2, for the CC, the 33-direction data is significantly lower than both the 55-direction and 64-direction data. The posterior body of the CC demonstrates a significant difference between the 55-direction and 64-direction datasets.

In figure 3, for the CST, there is a significant difference between the 64-direction data sets and the 55- and 33- direction data sets at the level of the superior corona radiata. No significant differences are seen between the 55- and 33-direction groups.

In figure 4, for the CB, the 55 direction data set is significantly higher than the 64-direction and 33-direction datasets for the majority of the tract. There are statistical difference between the 64- and 33-direction data sets anteriorly and posteriorly within the CB.

In figure 5, for the SLF, the 55 direction data set is significantly higher than the 64-direction and 33-direction datasets, while there is no significant difference between the 64- and 33-direction data.

In figure 6, for the ACR, significant differences are seen among all the datasets along the course of the entire tract.

In figure 7, for the UF, the 64 direction data set is significantly lower than the 55- and 33-direction data posteriorly. No significant differences are seen between the 55-direction and 33-direction data.

In contradistinction, Figures 8-13 illustrate the local variance measure for each cross-sectional ROI for the three groups of each white matter pathway. No significant differences were identified among the three groups for any cross-sectional ROI for each white matter pathway (i.e. $p > 0.05$ for all tracts and ROIs).

4. Discussion

It is widely disputed whether scan parameters influence DTI measurements such as FA. While it has been shown that the greater the number of gradient directions yield more accurate the FA measurement, it is known that there are limited improvements in accuracy beyond 30 gradient directions[37,38]. However, these studies compare the differences in FA measurement within the same scanner hardware and sequence, only varying the number of gradient directions. For example, Lebel et al. found that in an examination of 11 healthy volunteers collected on a 1.5T scanner for directions of 6, 30, and 60 found that even though the 6-direction data set proves to be comparable to the 30 and 60 directions, the greater the number of directions has its advantages in probabilistic tractography and resolving cross fibers[39]. However, other studies that suggest that parameters do not influence DTI measurements[40]. Ni et al. specifically found that the difference of parameters between 6 directions, 21 directions, and 31 directions had no effect on the FA values[40].

Our results suggest that there is a systemic impact on sequence parameters, such as gradient directions, slice thickness, and voxel size, and also hardware. Interestingly, the impact of sequence parameters and hardware vary for different white matter pathways and also cross sectional location within a tract. As a result, combining or comparing DTI datasets collected on different scanners or with different scan parameters would be methodologically invalid.

The variability that exists between different parameters poses a problem for comparing patients if large previously collected normal datasets do not exist. In order for there to be a comparable data set, the single subject must match to the control group in

demographics and co-morbidities. This is hard to do given the amount of variability that can occur between different subjects.

The results from this study suggest an alternate approach to assessing white matter integrity to the best of our knowledge not previously considered. Previously, studies use ROIs of different metrics such as FA and MD to define the white matter throughout the tract. Here we show that local variance of white matter integrity along the course of the tract demonstrates a degree of homogeneity and this homogeneity along the course of a tract appears scanner and sequence independent. Using this approach, no significant differences were found for any of the white matter tracts among the three data sets.

A prior study examined neighborhood-based texture measures[41]. Our studies are similar because we are both measuring within the gradient of the white matter tract instead of using scalar measures such as FA, MD, and RD. However, the neighborhood-based texture measure still requires a normal database for comparison. Given the relative homogeneity along the course of the tract demonstrated in our study in normal individuals, focal pathology will likely demonstrate a deviation from this relative homogeneity. As a result, it may be possible to apply this approach to single-subject analysis of focal or multi-focal disease without the need for a normative control database.

These results show that the degree of homogeneity of each tract is similar among datasets collected with varying sequence parameters and hardware (including vendor, head coil, and field strength). As a result, it may be possible to combine normative or research datasets across different platforms if the data is assessed in the fashion.

There are a number of limitations to note. First, the sample size is for the 33-direction data set is relatively small. Furthermore, the study would be optimized if the same patients were identical for all three datasets. The data analysis approach was chosen to mimic typical ROI analysis schemes; however, a more continuous measure along the course of the tract using tractography would yield more data and illustrate the degree of homogeneity continuously along the tract as opposed to evenly spaces cross sections.

Future directions include assessing the approach in a patient population and repeating the analysis in a prospective fashion on a larger normative dataset. These

studies will help elucidate if the local variance approach to DTI analysis is suitable for individual clinical use.

Figures and Tables

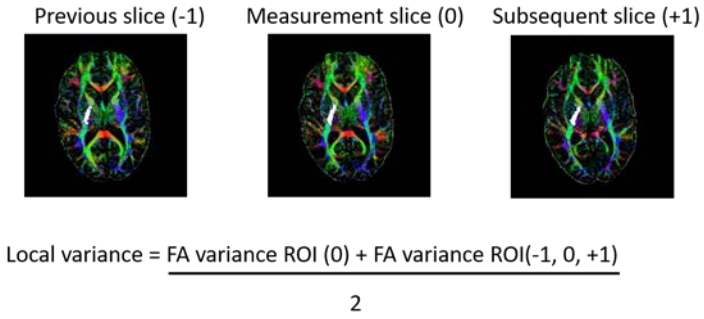

Figure 1: Description of how the local variance metric is calculated in this example of the local variance of the posterior limb of the internal capsule. The in-plane variance from the measurement slice is averaged with the out-of-plane variance measured by the ROIs of previous and subsequent slice.

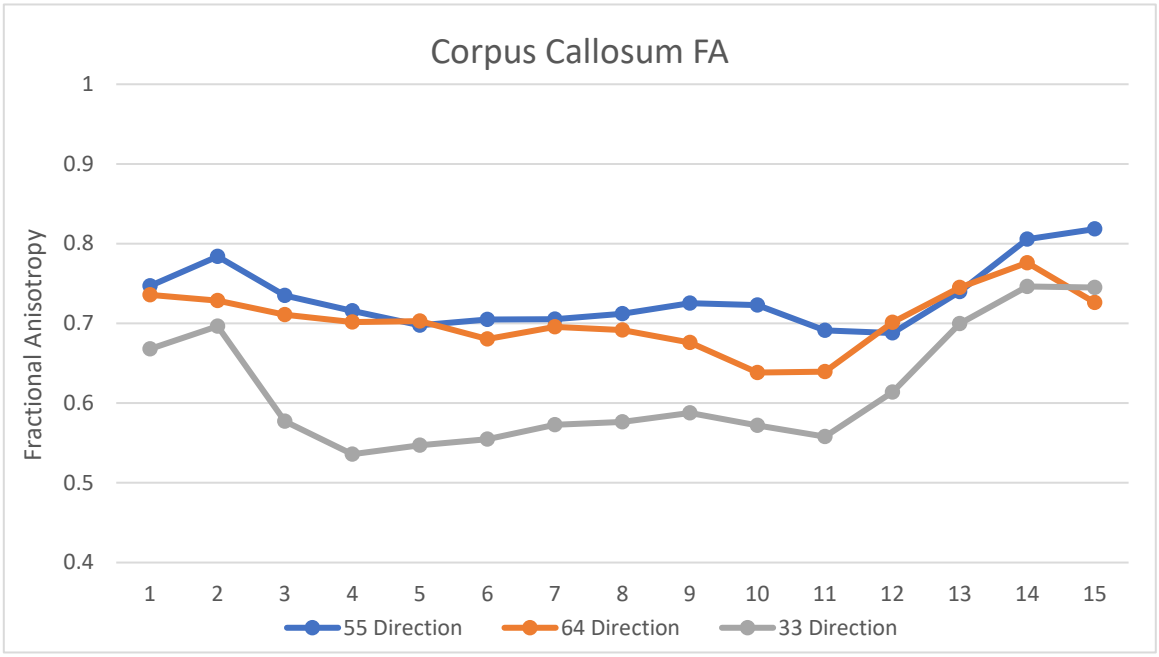

Figure 2: Plot of Fractional Anisotropy (FA) values within cross sections of the Corpus Callosum going anterior to posterior for each data set. The 33-direction data is significantly lower than both the 55-direction and 64-direction data. The posterior body of the CC demonstrates a significant difference between the 55-direction and 64-direction datasets.

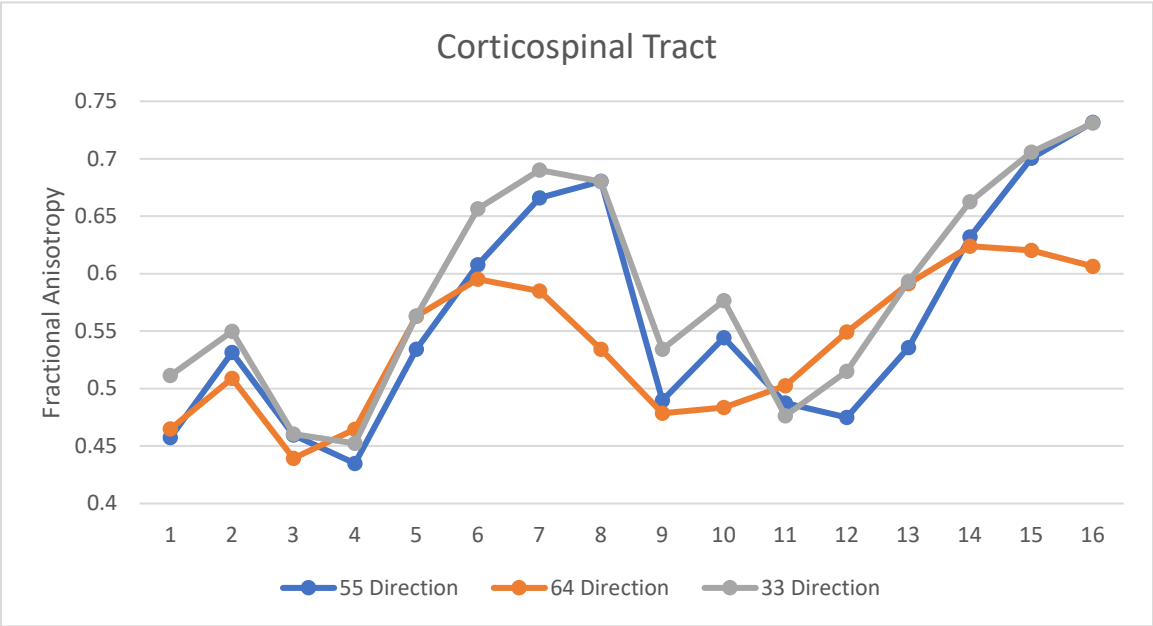

Figure 3: Plot of Fractional Anisotropy (FA) values within cross sections of the Corticospinal Tract going superior to inferior for each data set. There is a significant difference between the 64-direction data sets and the 55- and 33- direction data sets at the level of the superior corona radiata. No significant differences are seen between the 55- and 33-direction groups.

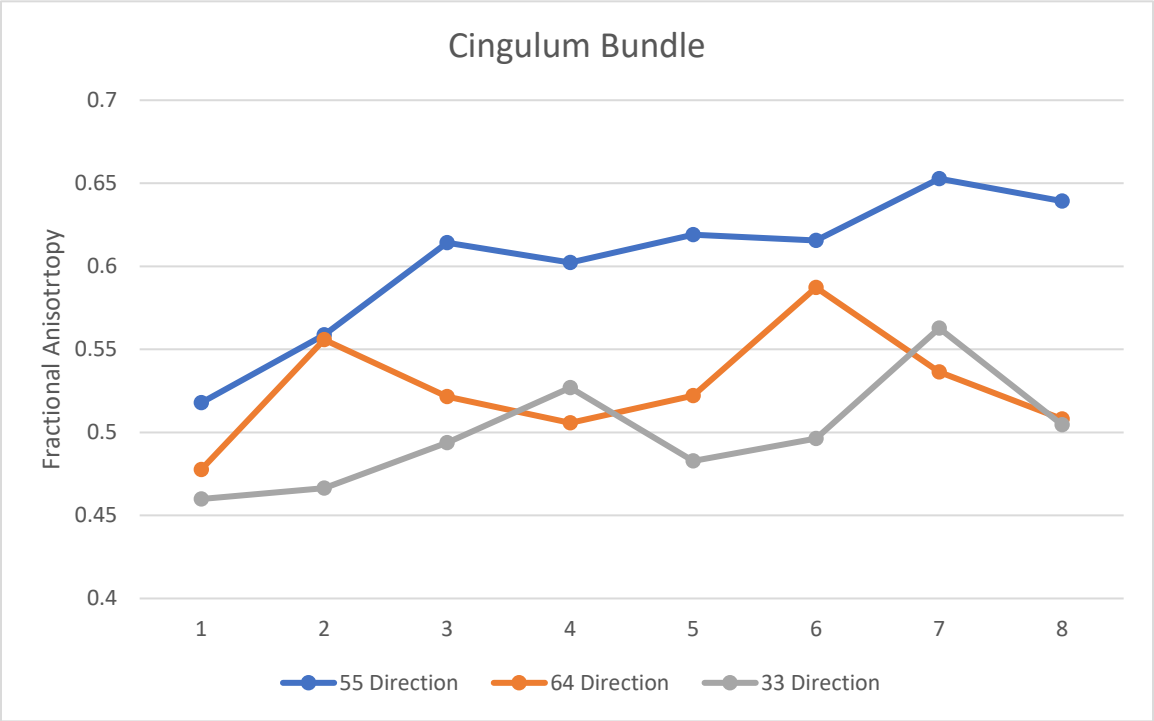

Figure 4: Plot of Fractional Anisotropy (FA) values within cross sections of the Cingulum Bundle (CB) going anterior to posterior for each data set. The 55 direction data set is significantly higher than the 64-direction and 33-direction datasets for the majority of the tract. There are statistical difference between the 64- and 33-direction data sets anteriorly and posteriorly within the CB.

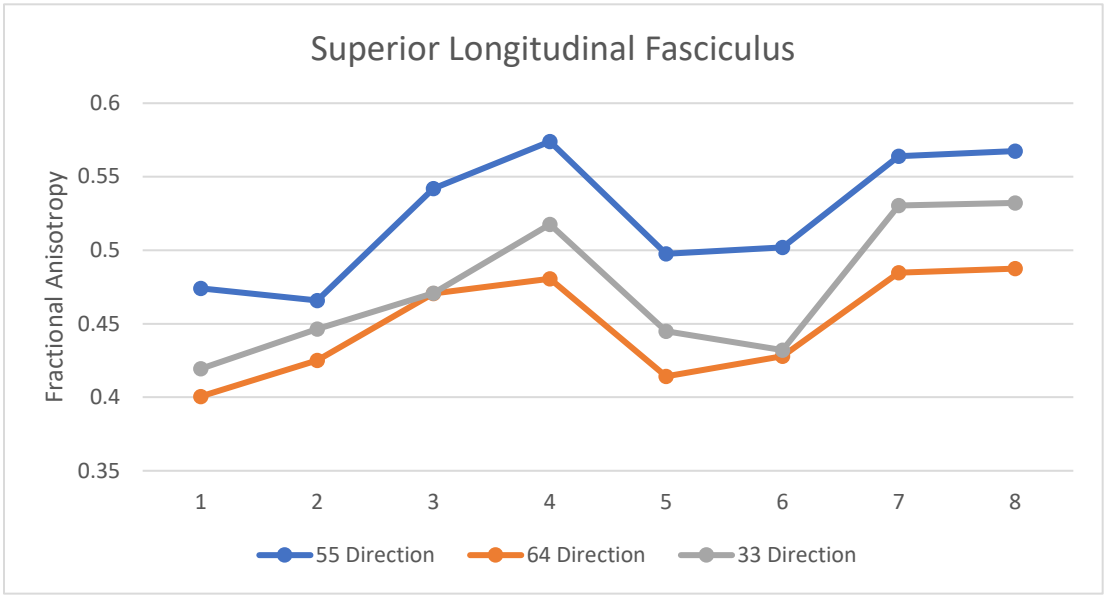

Figure 5: Plot of Fractional Anisotropy (FA) values within cross sections of the Superior Longitudinal Fasciculus (SLF) going anterior to posterior for each data set. The 55 direction data set is significantly higher than the 64-direction and 33-direction datasets, while there is no significant difference between the 64- and 33-direction data.

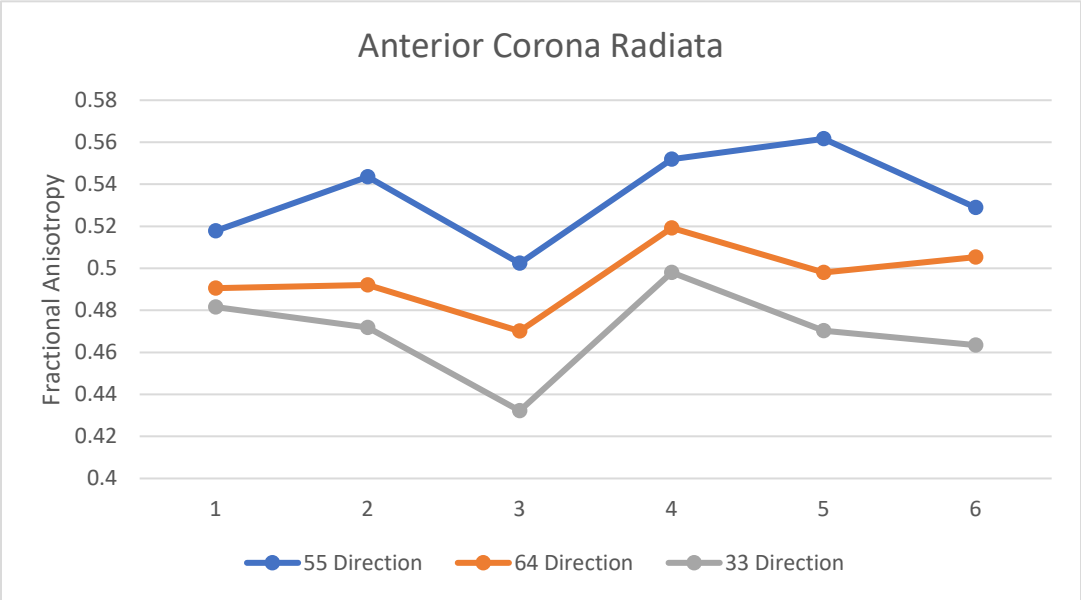

Figure 6: Plot of Fractional Anisotropy (FA) values within cross sections of the Anterior Corona Radiata (ACR) going anterior to posterior for each data set. Significant differences are seen among all the datasets along the course of the entire tract.

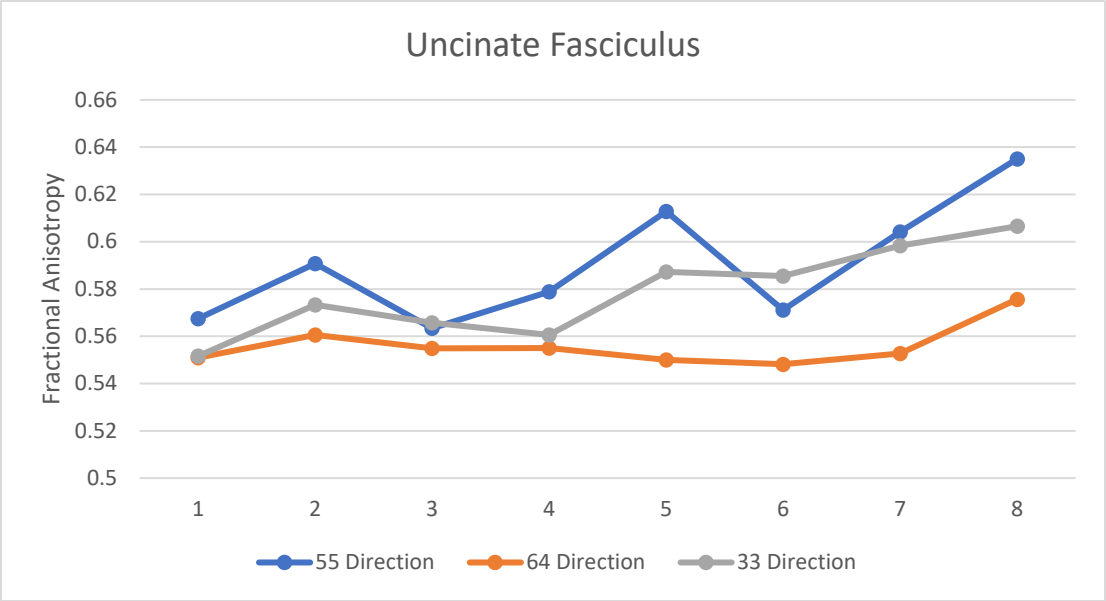

Figure 7: Plot of Fractional Anisotropy (FA) values within cross sections of the Uncinate Fasciculus (UF) going anterior to posterior for each data set. The 64 direction data set is significantly lower than the 55- and 33-direction data posteriorly. No significant difference are seen between the 55-direction and 33-direction data.

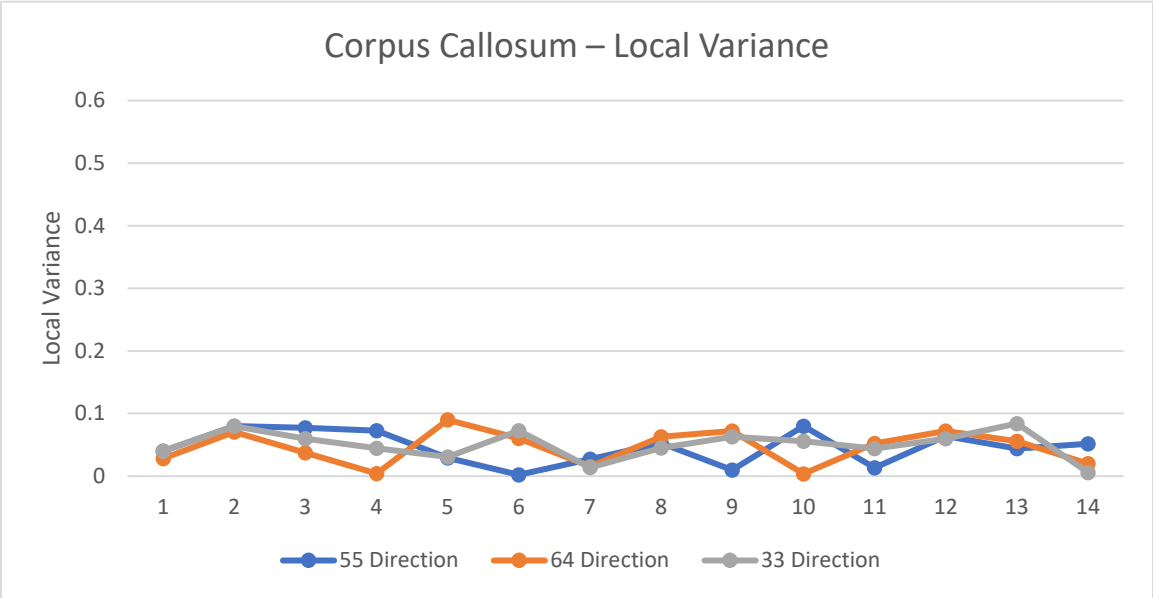

Figure 8: Plot of local variance across the Corpus Callosum

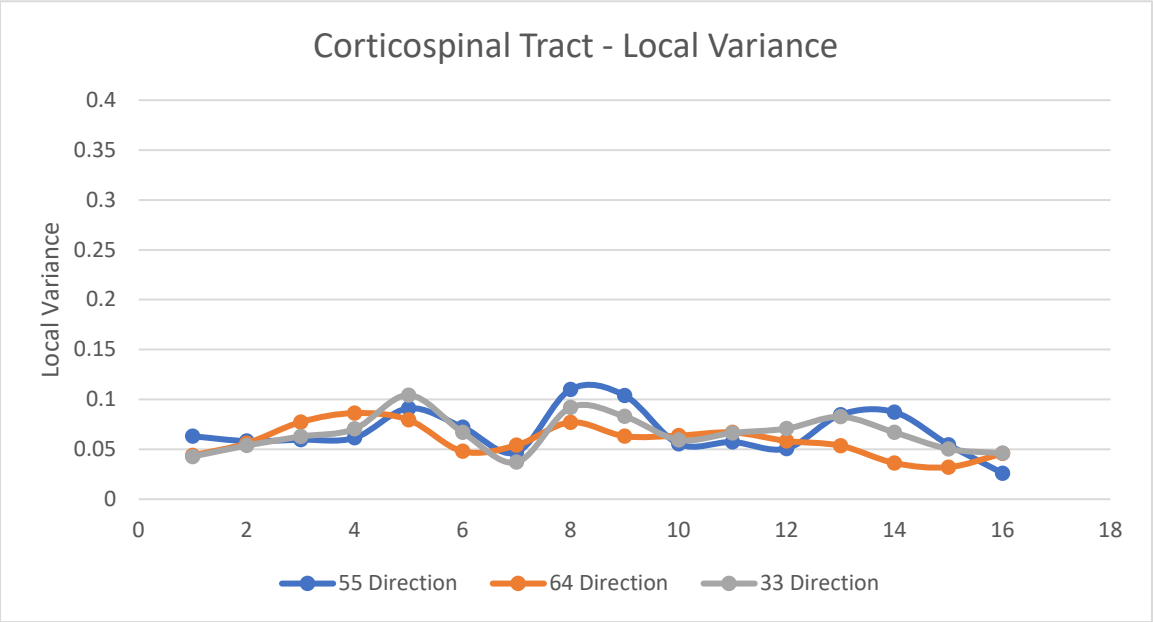

Figure 9: Plot of local variance across the Corticospinal tract

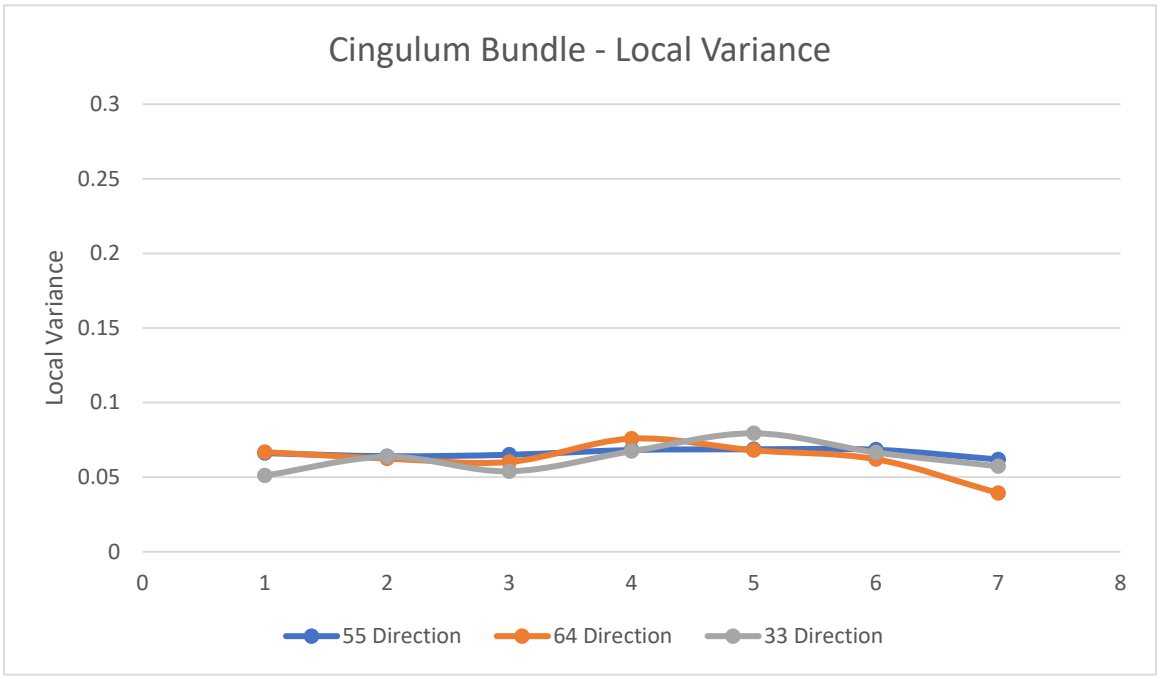

Figure 10: Plot of local variance across the Cingulum Bundle

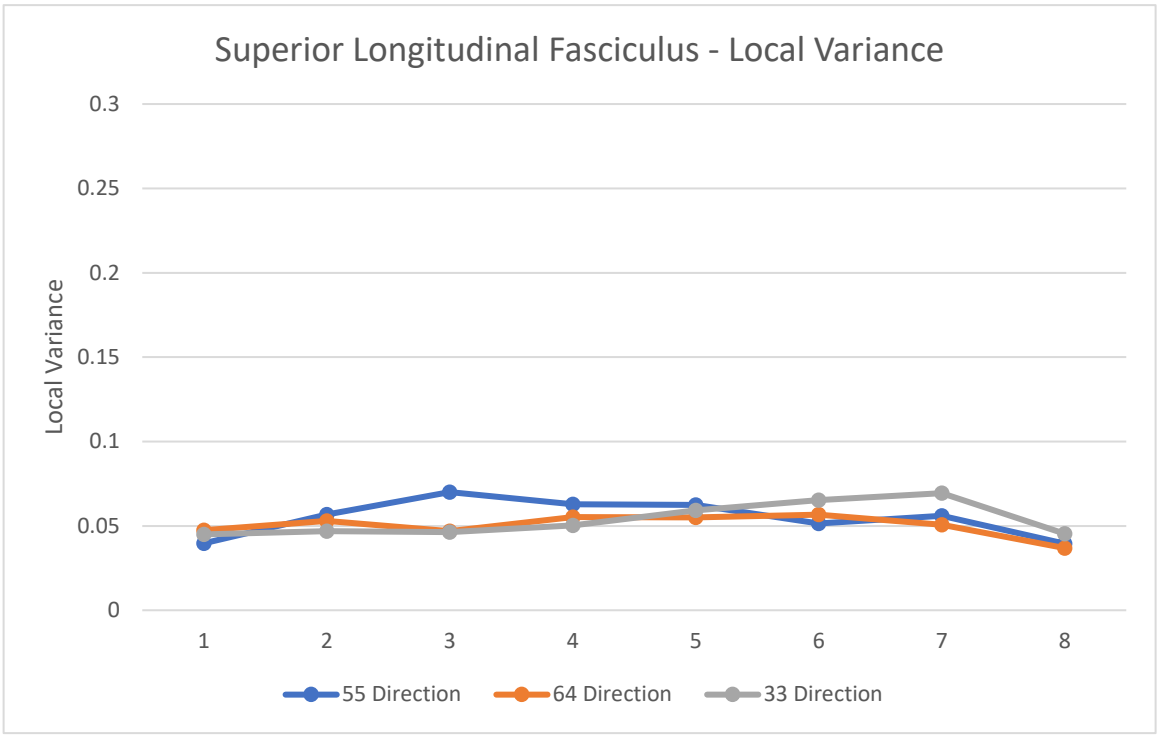

Figure 11: Plot of local variance across the Superior Longitudinal Fasciculus

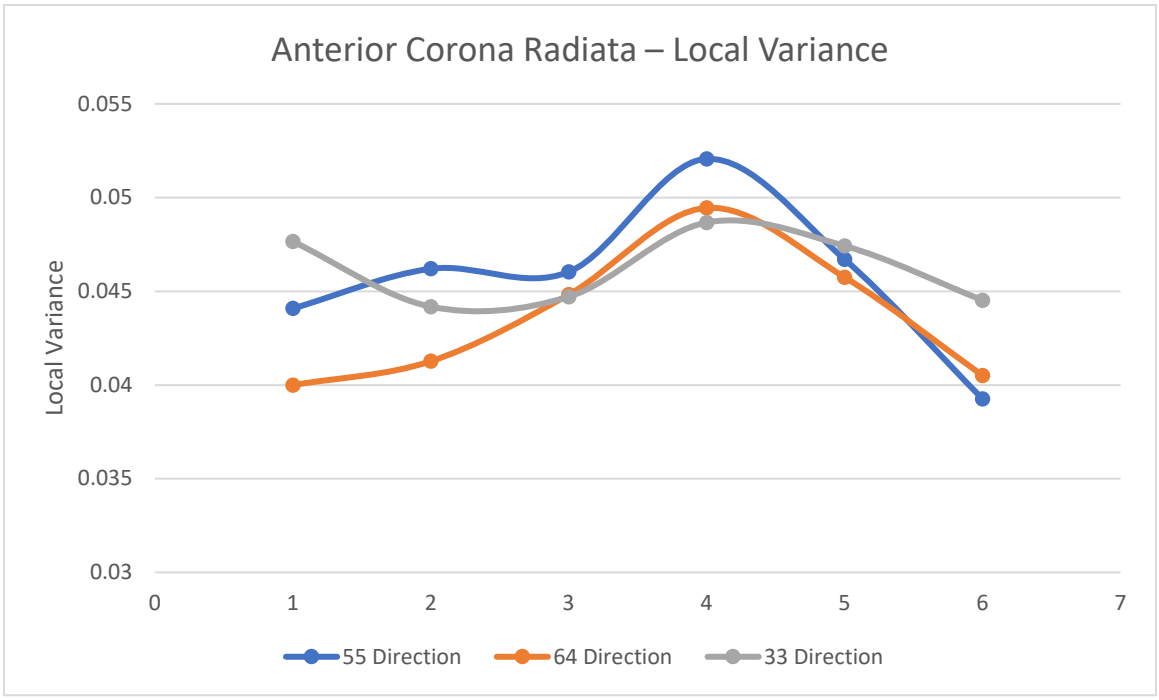

Figure 12: Plot of local variance across the Anterior Corona Radiata

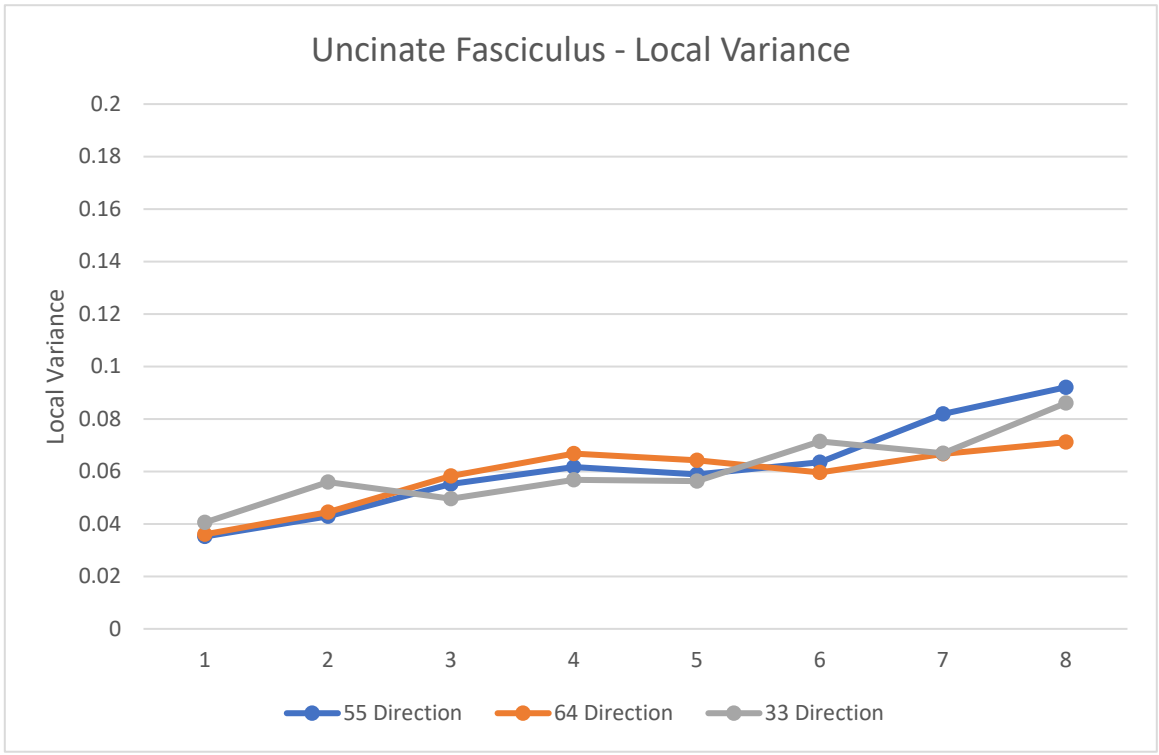

Figure 13: Plot of local variance across the Uncinate Fasciculus

Table 1
P-values for Corpus Callosum FA ROIs

	1	2	3	4	5	6	7	8	9	10	11	12	13	14	15
55 vs 33	0.00	0.01	0.00	0.00	0.00	0.00	0.00	0.00	0.00	0.00	0.00	0.04	0.18	0.00	0.08
55 vs 64	0.39	0.00	0.08	0.31	0.70	0.05	0.37	0.06	0.00	0.00	0.01	0.44	0.69	0.05	0.00
64 vs 33	0.00	0.26	0.00	0.00	0.00	0.00	0.00	0.00	0.00	0.01	0.01	0.02	0.12	0.13	0.61

Table 2
P-values for Corticospinal Tract FA ROIs

	1	2	3	4	5	6	7	8	9	10	11	12	13	14	15	16
55 vs 33	0.00	0.44	0.96	0.48	0.20	0.02	0.20	0.99	0.11	0.10	0.60	0.23	0.07	0.11	0.84	0.97
55 vs 64	0.59	0.07	0.16	0.07	0.04	0.36	0.00	0.00	0.48	0.00	0.31	0.00	0.00	0.46	0.00	0.00
64 vs 33	0.00	0.11	0.33	0.64	0.99	0.00	0.00	0.00	0.05	0.00	0.26	0.31	0.94	0.04	0.01	0.00

Table 3
P-values for Cingulum Bundle FA ROIs

	1	2	3	4	5	6	7	8
55 vs 33	0.15	0.00	0.01	0.05	0.00	0.04	0.02	0.00
55 vs 64	0.06	0.88	0.00	0.00	0.00	0.12	0.00	0.00
64 vs 33	0.62	0.00	0.49	0.53	0.01	0.09	0.40	0.90

Table 4
P-values for Superior Longitudinal Fasciculus FA ROIs

	1	2	3	4	5	6	7	8
55 vs 33	0.02	0.51	0.00	0.03	0.08	0.02	0.34	0.09
55 vs 64	0.00	0.00	0.00	0.00	0.00	0.00	0.00	0.00
64 vs 33	0.39	0.46	0.99	0.13	0.28	0.88	0.20	0.03

Table 5
P-values for Anterior Corona Radiata FA ROIs

	1	2	3	4	5	6
55 vs 33	0.33	0.02	0.00	0.12	0.01	0.04
55 vs 64	0.00	0.00	0.00	0.00	0.00	0.00
64 vs 33	0.72	0.44	0.48	0.89	0.43	0.40

Table 6
P-values for Uncinate Fasciculus FA ROIs

	1	2	3	4	5	6	7	8
55 vs 33	0.65	0.53	0.95	0.64	0.58	0.58	0.83	0.56
55 vs 64	0.03	0.00	0.42	0.05	0.00	0.05	0.00	0.00
64 vs 33	0.71	0.21	0.62	0.55	0.09	0.04	0.00	0.12

References:

1. Croteau-Chonka EC, Dean DC, Remer J, Dirks H, O'Muircheartaigh J, Deoni SCL. Examining the relationships between cortical maturation and white matter myelination throughout early childhood. *Neuroimage*. 2016;125:413-421. doi:10.1016/j.neuroimage.2015.10.038.
2. Thakur KT, Albanese E, Giannakopoulos P, et al. *Neurological Disorders*.; 2016. http://www.ncbi.nlm.nih.gov/pubmed/27227247. Accessed September 6, 2017.
3. Niogi SN, Mukherjee P. Diffusion tensor imaging of mild traumatic brain injury. *J Head Trauma Rehabil*. 2010;25(4):241-255. doi:10.1097/HTR.0b013e3181e52c2a.
4. Wintermark M, Sanelli PC, Anzai Y, et al. Imaging evidence and recommendations for traumatic brain injury: Advanced neuro- and neurovascular imaging techniques. *Am J Neuroradiol*. 2015;36(2):E1-E11. doi:10.3174/ajnr.A4181.
5. Welch RD, Ayaz SI, Lewis LM, et al. Ability of Serum Glial Fibrillary Acidic Protein, Ubiquitin C-Terminal Hydrolase-L1, and S100B To Differentiate Normal and Abnormal Head Computed Tomography Findings in Patients with Suspected Mild or Moderate Traumatic Brain Injury. *J Neurotrauma*. 2016;33(2):203-214. doi:10.1089/neu.2015.4149.
6. Scheid R, Preul C, Gruber O, Wiggins C, von Cramon DY. Diffuse axonal injury associated with chronic traumatic brain injury: evidence from T2*-weighted gradient-echo imaging at 3 T. *AJNR Am J Neuroradiol*. 24(6):1049-1056. http://www.ncbi.nlm.nih.gov/pubmed/12812926. Accessed September 25, 2017.
7. Niogi SN, Mukherjee P, Ghajar J, et al. Extent of microstructural white matter injury in postconcussive syndrome correlates with impaired cognitive reaction time: A 3T diffusion tensor imaging study of mild traumatic brain injury. *Am J Neuroradiol*. 2008;29(5). doi:10.3174/ajnr.A0970.
8. Niogi SN, Mukherjee P. Diffusion tensor imaging of mild traumatic brain injury. *J Head Trauma Rehabil*. 2010;25(4). doi:10.1097/HTR.0b013e3181e52c2a.
9. Shenton ME, Hamoda HM, Schneiderman JS, et al. A review of magnetic resonance imaging and diffusion tensor imaging findings in mild traumatic brain

injury. *Brain Imaging Behav*. 2012;6(2):137-192. doi:10.1007/s11682-012-9156-5.

10. Jones D, Cercignani M. Twenty-five pitfalls in the analysis of diffusion MRI data. *NMR Biomed*. 2010;23(7):803-820. doi:10.1002/nbm.1543.
11. Lerner A, Mogensen MA, Kim PE, Shiroishi MS, Hwang DH, Law M. Clinical Applications of Diffusion Tensor Imaging. *World Neurosurg*. August 2013. doi:10.1016/j.wneu.2013.07.083.
12. Song S, Sun S, Ju W, Lin S. Diffusion tensor imaging detects and differentiates axon and myelin degeneration in mouse optic nerve after retinal ischemia. *Neuroimage*. 2003;20(3):1714-1722. doi:10.1016/j.neuroimage.2003.07.005.
13. Nir TM, Jahanshad N, Villalon-Reina JE, et al. Effectiveness of regional DTI measures in distinguishing Alzheimer's disease, MCI, and normal aging. *NeuroImage Clin*. 2013;3:180-195. doi:10.1016/j.nicl.2013.07.006.
14. Douaud G, Jbabdi S, Behrens TEJ, et al. DTI measures in crossing-fibre areas: increased diffusion anisotropy reveals early white matter alteration in MCI and mild Alzheimer's disease. *Neuroimage*. 2011;55(3):880-890. doi:10.1016/j.neuroimage.2010.12.008.
15. Reas ET, Hagler DJ, White NS, et al. Sensitivity of restriction spectrum imaging to memory and neuropathology in Alzheimer's disease. *Alzheimers Res Ther*. 2017;9(1):55. doi:10.1186/s13195-017-0281-7.
16. Ishida T, Donishi T, Iwatani J, et al. Interhemispheric disconnectivity in the sensorimotor network in bipolar disorder revealed by functional connectivity and diffusion tensor imaging analysis. *Heliyon*. 2017;3(6):e00335. doi:10.1016/j.heliyon.2017.e00335.
17. Squarcina L, Houenou J, Altamura AC, Soares J, Brambilla P. Association of increased genotypes risk for bipolar disorder with brain white matter integrity investigated with tract-based spatial statistics. *J Affect Disord*. 2017;221:312-317. doi:10.1016/j.jad.2017.06.031.
18. Kurumaji A, Itasaka M, Uezato A, et al. A distinctive abnormality of diffusion tensor imaging parameters in the fornix of patients with bipolar II disorder. *Psychiatry Res Neuroimaging*. 2017;266:66-72. doi:10.1016/j.pscychresns.2017.06.005.

19. Onay A, Yapici Eser H, Ulasoglu Yildiz C, Aslan S, Tali ET. A combined VBM and DTI study of schizophrenia: bilateral decreased insula volume and cerebral white matter disintegrity corresponding to subinsular white matter projections unlinked to clinical symptomatology. *Diagnostic Interv Radiol*. 2017;23(5):390-397. doi:10.5152/dir.2017.16519.
20. Fox WC, Park MS, Belverud S, Klugh A, Rivet D, Tomlin JM. Contemporary imaging of mild TBI: the journey toward diffusion tensor imaging to assess neuronal damage. *Neurol Res*. 2013;35(3):223-232. doi:10.1179/1743132813Y.0000000162.
21. Mac Donald C, Johnson A, Cooper D, et al. Cerebellar white matter abnormalities following primary blast injury in US military personnel. *PLoS One*. 2013;8(2):e55823. doi:10.1371/journal.pone.0055823.
22. Wilde EA, Ayoub KW, Bigler ED, et al. Diffusion tensor imaging in moderate-to-severe pediatric traumatic brain injury: changes within an 18 month post-injury interval. *Brain Imaging Behav*. 2012;6(3):404-416. doi:10.1007/s11682-012-9150-y.
23. Niogi SN, Mukherjee P, Ghajar J, et al. Structural dissociation of attentional control and memory in adults with and without mild traumatic brain injury. *Brain*. 2008;131(12). doi:10.1093/brain/awn247.
24. Niogi SN, Mukherjee P, Ghajar J, et al. Extent of microstructural white matter injury in postconcussive syndrome correlates with impaired cognitive reaction time: a 3T diffusion tensor imaging study of mild traumatic brain injury. *AJNR Am J Neuroradiol*. 2008;29(5):967-973. doi:10.3174/ajnr.A0970.
25. Bendlin BB, Ries ML, Lazar M, et al. Longitudinal changes in patients with traumatic brain injury assessed with diffusion-tensor and volumetric imaging. *Neuroimage*. 2008;42(2):503-514. doi:10.1016/j.neuroimage.2008.04.254.
26. Kunz N, Zhang H, Vasung L, et al. Assessing white matter microstructure of the newborn with multi-shell diffusion MRI and biophysical compartment models. *Neuroimage*. 2014;96:288-299. doi:10.1016/j.neuroimage.2014.03.057.
27. Xu D, Mukherjee P, Barkovich a J. Pediatric brain injury: can DTI scalars predict functional outcome? *Pediatr Radiol*. 2013;43(1):55-59. doi:10.1007/s00247-012-

2481-4.

28. Schneider JFL, Il'yasov KA, Hennig J, Martin E. Fast quantitative diffusion-tensor imaging of cerebral white matter from the neonatal period to adolescence. *Neuroradiology*. 2004;46(4):258-266. doi:10.1007/s00234-003-1154-2.
29. Pfefferbaum A, Adalsteinsson E, Sullivan E V. Frontal circuitry degradation marks healthy adult aging: Evidence from diffusion tensor imaging. *Neuroimage*. 2005;26(3):891-899. doi:10.1016/j.neuroimage.2005.02.034.
30. Abe O, Aoki S, Hayashi N, et al. Normal aging in the central nervous system: quantitative MR diffusion-tensor analysis. *Neurobiol Aging*. 23(3):433-441. http://www.ncbi.nlm.nih.gov/pubmed/11959406. Accessed September 6, 2017.
31. Grieve SM, Williams LM, Paul RH, Clark CR, Gordon E. Cognitive aging, executive function, and fractional anisotropy: a diffusion tensor MR imaging study. *AJNR Am J Neuroradiol*. 2007;28(2):226-235. http://www.ncbi.nlm.nih.gov/pubmed/17296985. Accessed September 6, 2017.
32. Pfefferbaum A, Adalsteinsson E, Sullivan E V. Replicability of diffusion tensor imaging measurements of fractional anisotropy and trace in brain. *J Magn Reson Imaging*. 2003;18(4):427-433. doi:10.1002/jmri.10377.
33. Vollmar C, O'Muircheartaigh J, Barker GJ, et al. Identical, but not the same: intra-site and inter-site reproducibility of fractional anisotropy measures on two 3.0T scanners. *Neuroimage*. 2010;51(4):1384-1394. doi:10.1016/j.neuroimage.2010.03.046.
34. Alexander AL, Lee JE, Wu Y-C, Field AS. Comparison of Diffusion Tensor Imaging Measurements at 3.0 T versus 1.5 T with and without Parallel Imaging. *Neuroimaging Clin N Am*. 2006;16(2):299-309. doi:10.1016/j.nic.2006.02.006.
35. Smith SM, Jenkinson M, Woolrich MW, et al. Advances in functional and structural MR image analysis and implementation as FSL. *Neuroimage*. 2004;23:S208-S219. doi:10.1016/j.neuroimage.2004.07.051.
36. Niogi SN, Mukherjee P, McCandliss BD. Diffusion tensor imaging segmentation of white matter structures using a Reproducible Objective Quantification Scheme (ROQS). *Neuroimage*. 2007;35(1):166-174. doi:10.1016/j.neuroimage.2006.10.040.

37. Skare S, Hedehus M, Moseley ME, Li TQ. Condition number as a measure of noise performance of diffusion tensor data acquisition schemes with MRI. *J Magn Reson*. 2000;147(2):340-352. doi:10.1006/jmre.2000.2209.
38. Papadakis NG, Xing D, Huang CL-H, Hall LD, Carpenter TA. A Comparative Study of Acquisition Schemes for Diffusion Tensor Imaging Using MRI. *J Magn Reson*. 1999;137(1):67-82. doi:10.1006/jmre.1998.1673.
39. Lebel C, Benner T, Beaulieu C. Six is enough? Comparison of diffusion parameters measured using six or more diffusion-encoding gradient directions with deterministic tractography. *Magn Reson Med*. 2012;68(2):474-483. doi:10.1002/mrm.23254.
40. Ni H, Kavcic V, Zhu T, Ekholm S, Zhong J. Effects of number of diffusion gradient directions on derived diffusion tensor imaging indices in human brain. *AJNR Am J Neuroradiol*. 2006;27(8):1776-1781. http://www.ncbi.nlm.nih.gov/pubmed/16971635. Accessed September 6, 2017.
41. Thomsen FSL, Delrieux CA, de Luis-García R. Local texture descriptors for the assessment of differences in diffusion magnetic resonance imaging of the brain. *Int J Comput Assist Radiol Surg*. 2017;12(3):389-398. doi:10.1007/s11548-016-1505-1.